chemosensors

MDPI

Article

A Biomimetic Chip with Dendrimer-Encapsulated Platinum Nanoparticles for Enhanced Electrochemiluminescence Detection of Cardiac Troponin I †

Yun Hui [1], Weijun Kong [1], Weiliang Shu [1], Zhiting Peng [2], Fengshan Shen [1], Mingyang Jiang [1], Zhen Xu [1,*], Tianzhun Wu [1,*], Wenhua Zhou [1] and Xue-Feng Yu [1,*]

[1] Shenzhen Institute of Advanced Technology, Chinese Academy of Sciences, Shenzhen 518055, China
[2] Department of Ophthalmology, Li Ka Shing Faculty of Medicine, The University of Hong Kong, Hong Kong SAR, China
* Correspondence: zhen.xu@siat.ac.cn (Z.X.); 18665928630@wo.cn (T.W.); xf.yu@siat.ac.cn (X.-F.Y.)
† This paper is an extended version of our paper published in Hui, Y., Shu, W., Zhu, J., Li, J., Wu, T., Zhou, W., & Yu, X. Pt Dendrimer-Encapsulated Nanoparticles Modified UMEAs for Electrochemi-luminescence Heterogeneous Immunoassay. In Proceedings of 2023 IEEE SENSORS (pp. 1–4). IEEE, held in Vienna, Austria, 29 October 2023–1 November 2023.

Abstract: The measurement of cardiac troponin I (cTnI) is of vital importance for the early diagnosis of acute myocardial infarction. In this study, an enhanced electrochemiluminescent immunoassay for the highly sensitive and precise determination of cTnI was reported. A biomimetic chip with nepenthes peristome surface microstructures to achieve single-layer microbead arrays and integrated microelectrode arrays (MEAs) for ECL detection was microfabricated. Ru@SiO_2 nanoparticles were prepared as signal amplificators labeling immunomagnetic beads. Dendrimer-encapsulated platinum nanoparticles (Pt DENs) were electrochemically modified on ITO MEAs. The resulting Pt DEN-modified ITO MEAs preserved good optical transparency and exhibited an approximately 20-fold ECL signal amplification compared to that obtained from bare ITO. The method made full use of the biomimetic chip with Pt DENs to develop single-layer immunomagnetic bead arrays with increasingly catalyzed electrochemical oxidation of the $[Ru(bpy)_3]^{2+}$–TPA system. Consequently, a limit of detection calculated as 0.38 pg/mL (S/N = 3) was obtained with excellent selectivity, demonstrating significant potential for the detection of cTnI in clinical diagnostics.

Keywords: electrochemiluminescence immunosensor; Pt dendrimer-encapsulated nanoparticles; biomimetic nepenthes peristome structure; cardiac troponin I

Citation: Hui, Y.; Kong, W.; Shu, W.; Peng, Z.; Shen, F.; Jiang, M.; Xu, Z.; Wu, T.; Zhou, W.; Yu, X.-F. A Biomimetic Chip with Dendrimer-Encapsulated Platinum Nanoparticles for Enhanced Electrochemiluminescence Detection of Cardiac Troponin I. *Chemosensors* **2024**, *12*, 214. https://doi.org/10.3390/chemosensors12100214

Received: 4 September 2024
Revised: 3 October 2024
Accepted: 14 October 2024
Published: 16 October 2024

1. Introduction

The detection and quantification of protein biomarkers as a tool for medical decisions is of utmost importance for in vitro diagnostics. Taking cardiac troponin I (cTnI) as an example, the accurate detection of cTnI is crucial for the early diagnosis of acute myocardial infarction [1,2]. In recent decades, magneto-immunoassays utilizing magnetic microbeads have been recommended as favorable candidates for disease diagnostic thanks to their low cost, high sensitivity, excellent anti-interference ability, and easy automation [3].

Electrogenerated chemiluminescence, also called electrochemiluminescence (ECL), is advantageous because it can increase sensitivity and widen the dynamic range with nearly zero background noise; it has superior temporal and spatial control of light emission and preserves the simplicity, stability, and facility of the device [4–6]. Many researchers have utilized magneto-immunoassays in combination with ECL detection technology for the quantification of multiple biomarkers. For example, cobas e immunoassay analyzers are commercially available from Roche Diagnostics with a typical coupling of $[Ru(bpy)_3]^{2+}$ label and a TPA coreactant. Magneto-electrochemiluminescence immunoassays have been

widely investigated due to their significant advantages in preconcentration and separation of targets in complex samples and their feasibility in high-throughput analysis [7,8]. Recently, MBs have been used not only as support materials and separation tools through the specific molecular recognition but also as the signal labels to increase the detection sensitivity [9] However, as for the magnetic bead-based ECL immunoassay using the $[Ru(bpy)_3]^{2+}$–TPA system, $[Ru(bpy)_3]^{2+}$ immobilized on the magnetic beads (MBs) is positioned at a distance from the electrode, preventing direct electron transfer. ECL is generated several microns above the electrode surface, depending upon the oxidation and reduction processes involving TPA+* and TPA*, respectively, and their subsequent diffusion towards the electrode [10]. Moreover, it was observed that MBs generally aggregated and easily piled up on the electrode with magnets placed under the electrode, leading to a decrease in the ECL sensing signal. Thus, it is of vital importance to develop single-layer immunomagnetic [11] beads (IMBs) at the vicinity of the electrode surface and excellent electrode modification for improved electrooxidation of TPA [12]. On one hand, there have recently been some reports on manufactured magnetic microstructures for precisely controlling the magnetic field gradient to manipulate IMB arrays close to the electrode surface with the enhancement of both electrochemical and ECL signals. However, actively manipulating massive submicron beads to develop monodispersed arrays needs tedious operations or external setup, such as optical tweezers and dielectrophoretic and magnetic fields [13,14]. Many microfluidic chips with a microwell array [15], micropillar array [16], and "V"-shaped enclosure arrays [17] can capture large-scale and single-dispersion IMB arrays, but they exhibit relatively low efficiency and have difficulty in integrating with ECL electrodes. Our group previously investigated biomimetic nepenthes peristome surfaces (NPS) with unique capillary phenomena and spontaneously directional liquid transport for rapidly large-scale and single-layer microbead arrays [18]. And high-density trapping of microparticles (down to 5 μm in diameter) were realized by making use of the curvature-induced Laplace pressure effect for a fluorescent enzyme-linked immunoassay [19]. On the other hand, indium tin oxide (ITO) serves a dual purpose as both the substrate for the biomimetic chip for bead arrays and the working electrode in the ECL system. Given the sluggish kinetics of TPA on the ITO electrode, novel nanomaterials with high electrooxidation of TPA are necessary to improve the ECL performance. For example, carbon nanotubes (CNTs) were inserted by Valenti et al. as an interlayer between the luminophore and the MBs, to obtain a significant improvement of the ECL signal [20]. Metal nanoparticles encapsulated in PAMAM dendrimers are another good candidate to enhance the ECL signal in the biomarker assay [21]. Furthermore, dendrimer-encapsulated platinum nanoparticles (Pt DEN) can be electrochemically prepared on a transparent ITO electrode with dramatically enhanced ECL emission for the $[Ru(bpy)_3]^{2+}$/TPA system [22]. Hence, it is used in our study in combination with $[Ru(bpy)_3]^{2+}$-doped silica ($Ru@SiO_2$) nanoparticles, which are loaded in a high concentration of $[Ru(bpy)_3]^{2+}$ [23,24]. Herein, an ECL magneto-immunoassay with dendrimer-encapsulated Pt nanoparticle-modified biomimetic surfaces was proposed for the enhanced ECL detection of biomarker proteins. A schematic illustration of the workflow is shown in Figure 1. IMBs with different concentrations of analyte are first constructed via chemical and immunological reaction. Then, single-layer IMBs arrays with close distance to the electrode are developed on a biomimetic chip, owing to the curvature-induced Laplace pressure in the slipping mode and the evaporation-driven Marangoni effect in the climbing mode, respectively. Finally, Pt DEN-modified ITO microelectrode arrays (MEAs) are utilized to achieve a highly enhanced and stable ECL response for the determination of cTnI. This platform presents a promising alternative approach for the accurate and selective quantitative analysis of cTnI, which is crucial for the early diagnosis of acute myocardial infarction. Additionally, the results underscore the significant potential of biomimetic chips as platforms for investigating ECL imaging of large quantities of IMBs.

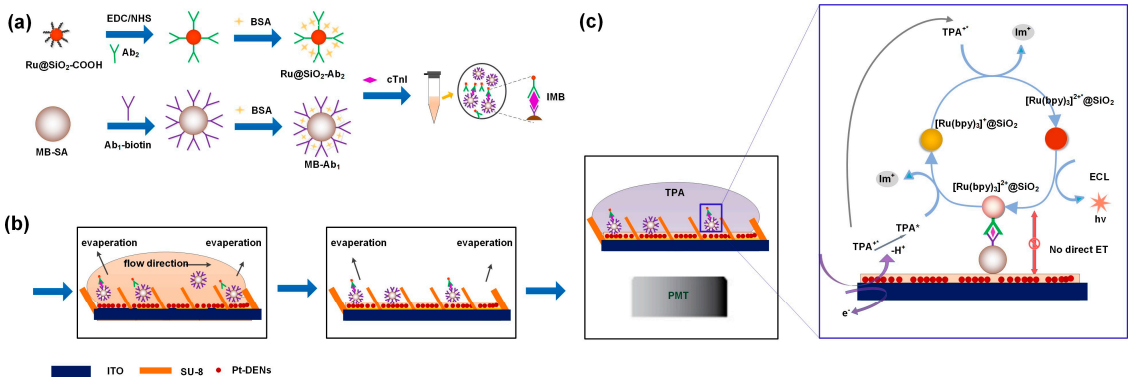

Figure 1. Schematic illustration of the workflow of the ECL magneto-sensing platform. (**a**) IMBs with $Ru@SiO_2$ nanoparticles as luminophores are prepared. (**b**) IMBs are loaded on the Pt-DEN-modified biomimetic NPE surfaces. (**c**) The ECL emission signal is collected by the photomultiplier tube (PMT) under the transparent electrode.

2. Materials and Methods

2.1. Materials and Apparatus

Tris(2,2j-bipyridyl)dichlororuthenium(II) hexahydrate tripropylamine (TPA), N-Hydroxysulfos sodium salt (sulfo-NHS), bovine serum albumin (BSA), 1-ethyl-3-(3-dimethylaminopropyl) carbodiimide (EDC), tween-20, and cellulose dialysis sacks (MW cutoff of 12,000) were purchased from Sigma-Aldrich (St. Louis, MO, USA). N-hexanol, cyclohexane and ammonium hydroxide (25 wt%), MES hydrate, 3-(Triethoxysilyl)propylsuccinic anhydride, tetraethyl orthosilicate, tetraethyl orthosilicate (TEOS, >99.9%), K_2PtCl_4, $NaBH_4$, and $LiClO_4$ were obtained from Aladdin Co., Ltd. (Shanghai, China). HCl, H_2SO_4, NaOH, H_2O_2, ethanol, and acetone were obtained from Shanghai Chemical Reagent Company (Shanghai, China). Amine-terminated sixth-generation PAMAM (G6-NH2 PAMAM) dendrimers were obtained from Chenyuan Co. (Weihai, China). The DynabeadsTM streptavidin trial kit was purchased from Invitrogen (Oslo, Norway). All of the reagents were of analytical grade. ITO-coated coverslips (22 × 40 mm, transmittance > 88% between 580 nm and 700 nm) with 15–30 ohm resistivity were provided by Human Troponin I-Cardiac (cTnI), and its mouse anti-human cTnI antibody (Biotin anti-cTnI antibody Ab_1, coating Ab_2) was purchased from Linc-Bio Science Co., Ltd. (Shanghai, China), as were the purified recombinant Troponin T-Cardiac (cTnT), myoglobin (Myo) antigen, human serum albumin (HSA), and carcinoembryonic antigen (CEA). SU-8 was obtained from MicroChem Corp Company (Westborough, MA, USA). Phosphate buffered saline (PBS) was purchased from Gibco (Waltham, MA, USA). Deionized water (DI, 18.2 MΩ) was used in all the experiments. UV-vis absorption spectra were determined using a spectrophotometer (Shimadzu, UV-2700, Kyoto, Japan) in a 1 cm quartz cell. The field emission scanning electron microscope (FESEM, Zeiss Sigma 300, Oberkochen, Germany) was used to observe the morphology of the samples. Transmission electron microscope (TEM) images were obtained using a JEM-3010 transmission electron microscope (JEOL Co., Ltd., Tokyo, Japan). Zeta potential (ζ-potential) analysis was performed with a Nano-Zetasizer (Malvern Instruments Ltd., Worcestershire, UK). All the electrochemical measurements, including cyclic voltammetry (CV) and chronoamperometry, were performed with the Reference 600 workstation (Gamry Instruments Co., Ltd., Warminster, PA, USA).

A platinum foil electrode was used as the counter electrode and a saturated Ag/AgCl as the reference electrode. The ECL intensity was measured using an ultraweak luminescence analyzer (MPI-H, Xi'an Remax Electronic Science & Technology Co., Ltd., Xi'an, China), and the PMT was placed at the bottom.

2.2. Fabrication of the Biomimetic Chip

In the previous reports, Nepenthes peristome microstructures (Figure 2a) have been studied with unique capillary phenomena. The design criteria for the biomimetic chip with nepenthes peristome microstructures for developing 5 μm microbead arrays are presented [19] and illustrated in Supplementary Materials Figure S1. To fabricate arrays for 2.8 μm microbeads, the biomimetic chip was manufactured with a smaller size and larger oblique angle, as is shown in Figure 2b. The fabrication process of the biomimetic nepenthes peristome microstructures is exhibited in Figure 2c. Initially, to increase adhesion to the photoresist, the ITO substrate was exposed to heating in a closed oven to 120 °C and plasma treatment for 5 min. Subsequently, SU-8 3005 was spun at 500 rpm for 10 s and then at 4000 rpm for 30 s. Following a soft bake, the oblique exposure with a dose of 50 mJ/cm^2 was performed, with the angle between the light path and the horizontal plane being arccos (52/77). The chip was then subjected to a post-exposure bake on a hotplate at 65 °C for 1 min and 95 °C for 2 min. The chip was subsequently soaked in SU-8 developer solution and developed at room temperature for 1 min, along with ultrasonic treatment for 4 s. The developing solution was removed by washing with ethanol. At this stage, semi-ellipsoidal inclined microwell arrays were successfully formed on the ITO substrate.

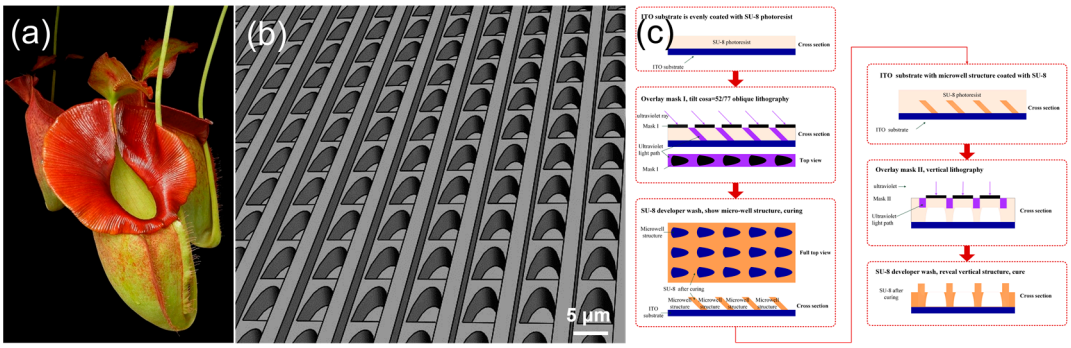

Figure 2. (**a**) Image of a pitcher plant (nepenthes), where the orange area is the peristome microstructures. (**b**) Illustration of the biomimetic NPS design for 2.8 μm size microparticle trapping. (**c**) Fabrication process of the biomimetic nepenthes peristome microstructures.

2.3. Synthesis of Pt-DENs

The synthesis of Pt-DENs followed a modified protocol based on previous research [22] with reduced half amounts of K_2PtCl_4 and $NaBH_4$. Initially, reagent bottles were immersed in aqua regia for six hours and subsequently rinsed with deionized water. Subsequently, 50 μL of 200 mM K_2PtCl_4 was added to 5 mL of a 10 μM G6NH_2-PAMAM aqueous solution. The pH of the resulting mixture was adjusted to 5.0 using a 10% HCl solution, and the solution was stirred for 76 h to ensure the complexation of platinum ions with the dendrimer's amine groups. Next, a chilled $NaBH_4$ solution (0.2 mL of 7.566 mg) was prepared, equivalent to 20 times the molar amount of platinum chloride, and it was gradually added to the mixture under vigorous stirring. The pH of the mixture was then adjusted to between 7 and 8, and the solution was maintained in a sealed vial for 24 h. Finally, the synthesized Pt-DEN solution was dialyzed using a cellulose dialysis bag with a molecular weight cut-off of 12,000 to 14,000 Daltons for 24 h to remove any impurities.

2.4. Preparation of Immunomagnetic Beads

For the highly specific and sensitive detection of target proteins, we designed a classical sandwich of immunomagnetic beads (IMBs) utilizing two functionalized components: primary antibody-modified magnetic beads (MB-Ab_1) and secondary antibody-modified quantum dot nanoparticles (Ru@SiO_2–Ab_2). Magnetic beads (MBs) have been extensively used in immunoassays due to their efficient dispersion capability, simplified separation steps, and effective magnetic pre-enrichment of low-abundance analytes in complex ma-

trices. Ultra-bright Ru@SiO_2, filled with large amounts of [Ru(bpy)$_3$]2+, functions as ECL labels that record optical information regarding antigen concentrations. The preparation of sandwich IMBs involves three steps: the preparation of MB-Ab_1 bioconjugate, the preparation of Ru@SiO_2–Ab_2 bioconjugate, and the assembly of sandwich IMBs, which are detailed in our previous work [25]. The modification of ITO MEAs with the Pt-DEN chemical reduction of the aqueous G6 PAMAM-OH (Pt2+) complexes with excess $NaBH_4$ produced a solution containing Pt-DENs. The biomimetic chip with ITO MEAs underwent 2 min plasma cleaning at medium power. Subsequently, the electrode was introduced to a freshly prepared solution of 10 μM Pt-DENs containing 0.1 M $LiClO_4$. A cyclic potential was then applied to the electrode three times, ranging between 1.20 and 1.75 V (vs. Ag/AgCl), with the scan rate of 10 mV/s. After electrochemical grafting of the Pt-DENs, the modified ITO MEAs were rinsed with deionized water and air-dried.

2.5. On-Chip Immunoassay Operation

ECL signals for various concentrations of cTnI antigen were recorded using an ultra-weak luminescence analyzer (MPI-H, Xi'an Remax Electronic Science Technology Co., Ltd., Xi'an, China), with potentials applied synchronously via an electrochemical Reference 600 workstation (Gamry Instruments Co., Ltd., Warminster, PA, USA). All the electrochemical measurements were conducted using a three-electrode system, comprising the fabricated chip with a Pt-DENs-modified ITO MEA electrode as the working electrode, a Pt wire as the counter electrode, and an Ag/AgCl reference electrode. Cyclic voltammetry (CV) measurements in solutions containing cTnI were performed at a scanning rate of 100 mV/s, within the potential range of 0 V to 1.40 V (vs. Ag/AgCl). The voltage of the photomultiplier tube (PMT), placed at the bottom of the analyzer, was set to 600 V.

3. Results and Discussion

3.1. Characterization of the Fabricated Biomimetic Microstructures

Scanning electron microscope (SEM, Zeiss Sigma 300, Oberkochen, Germany) images of the micro- fabricated biomimetic microstructures with semielliptical oblique microcavities with an oblique angle (arccos 52/77) are shown in Figure 3a. The enlarged cross-section view indicates that the semi-ellipsoidal inclined microwell arrays are developed on the ITO substrate, and the long semi-axis and the short semi-axis of the ellipse are 2 μm and 7 μm, respectively. The substrate of the biomimetic NPE structures is integrated with the MEAs. MEAs have been proven to be beneficial for ECL systems with fast electron transport and high current response [26,27]. The MEAs were characterized by cyclic voltammetry in a 5 mM ferricyanide solution containing 0.1 M KCl (Figure 3b). As anticipated, the electrochemical behavior of the MEAs varied significantly with the bulk electrode. The common ITO bulk electrode produced a peak-shaped voltammogram, while ITO MEA exhibited a sigmoidal curve, indicative of hemispherical diffusion of ferricyanide towards the working microelectrode surface. Figure 3c shows the bright-field microscope image of the trapped IMB arrays on the biomimetic chip. By incorporating the functional elements of biomimetic nepenthes peristome structures (NPS), a series of semielliptical oblique microcavities were positioned within the parallel microchannel. By leveraging the capillary effect, the parallel microgroove evenly distributed particles along the microchannel, while the semielliptical oblique microcavities accurately captured individual IMBs in a specific tilted direction. The tilted evaporation conditions used on a similar structure were set with the contact angle of 11° and tilt angle of −5°, based on our previous study [19]. The coverage rate of 2.8 μm IMBs is estimated to be about 40%, which is attributed to the curvature-induced Laplace pressure in the slipping mode and the evaporation-driven Marangoni effect in the climbing mode, respectively [28].

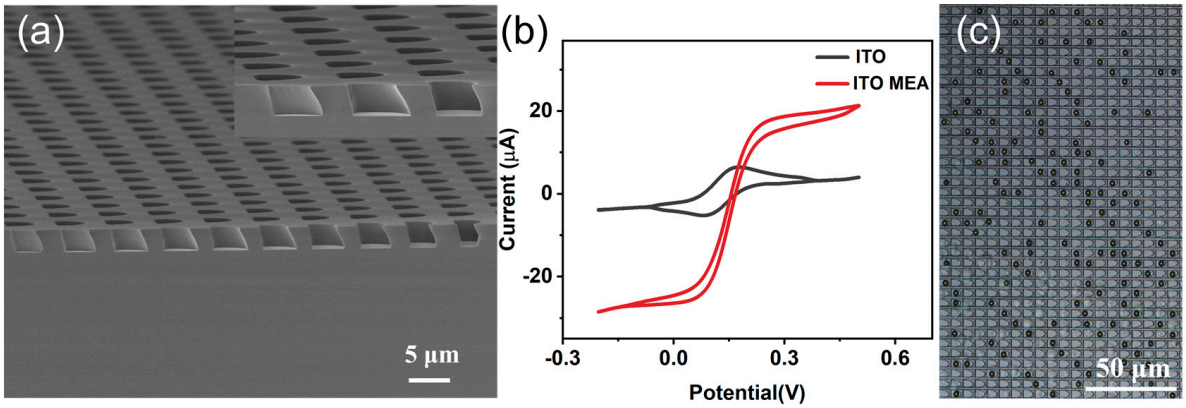

Figure 3. (**a**) SEM images for the cross-section view of semielliptical oblique microcavities. (**b**) CV curves of 5 mM ferricyanide on the bulk ITO electrode and ITO MEA at a scan rate of 50 mV s^{-1}. (**c**) Bright-field microscope image of trapped IMB array on the biomimetic surfaces.

3.2. Characterization of the Prepared Pt-DENs

The morphology, size, and absorbance spectrum of the Pt-DENs were monitored using transmission electron microscopy (TEM) and UV–visible techniques. As shown in Figure 4a, TEM images of the Pt-DENs revealed that the nanoparticles were monodispersed and approximately spherical, indicating that the Pt-DENs were stably encapsulated by dendrimers, as reported previously [22]. The average size of the Pt-DENs was approximately 1.88 nm, according to the statistical data of the particle size measured with ImageJ software (version 1.51j8, National Institutes of Health, Bethesda, MD, USA). And the inset figure shows that the lattice size was measured to be about 0.222 nm. Figure 4b shows the UV-vis absorbance spectrum of the Pt-DEN solution after a 2 h reduction. It was found that wavelengths greater than 300 nm had broad and featureless absorption lines, which is consistent with the formation of colloidal platinum [29] and indicates the formation of Pt DENs. There is a peak near 265 nm that may originate from the unreduced part that is still bound to the amine group in the dendrimer Pt^{2+}. Furthermore, the optical transmittance of bare ITO and Pt-DENs/ITO was measured to be approximately 88.65% and 82.45%, respectively, in the wavelength range of 580 nm to 700 nm. In comparison to bare ITO, Pt-DEN-modified ITO exhibited platinum-characteristic redox waves, including hydrogen adsorption/desorption, Pt surface oxidation, and the corresponding oxide reduction, as illustrated in Figure 4c. This observation confirms the successful generation of Pt-DENs on the electrode surfaces.

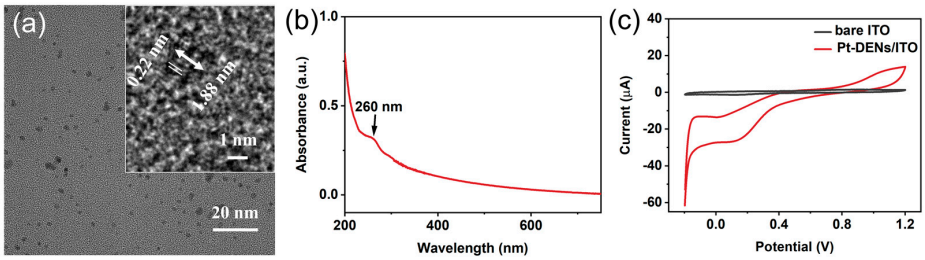

Figure 4. (**a**) TEM images of as-synthesized Pt-DENs. (**b**) UV-vis absorption spectroscopy of prepared Pt-DENs. (**c**) The electrochemical behavior of Pt-DEN-modified ITO and bare ITO electrode in the presence of 5 mM H2SO4 solutions.

3.3. Characterization and Optimization of Ru@SiO_2

The absorbance spectrum and morphology of the Ru@SiO_2 nanoparticles were characterized using UV–visible spectroscopy and scanning electron microscopy (SEM). The successful loading of $Ru(bpy)_3^{2+}$ into the SiO_2 NPs is demonstrated by the absorbance spectra in Figure 5a. Distinct peaks are observed at approximately 292 nm and 476 nm,

which correspond to the π–π^* electronic transition of bipyridine and metal-to-ligand charge transfer absorption, respectively. A slight red shift of the bipyridine absorbance peak is noted for the carboxylated Ru@SiO_2. Furthermore, the Ru@SiO_2 NPs exhibit a uniform, stable spherical structure with an average diameter of approximately 64 nm. The preparation condition of Ru@SiO_2 loaded with different concentrations of $Ru(bpy)_3^{2+}$ was optimized. It is observed in Figure 5b that the highest ECL response is obtained from Ru@SiO_2 loaded with 40 mM $Ru(bpy)_3^{2+}$.

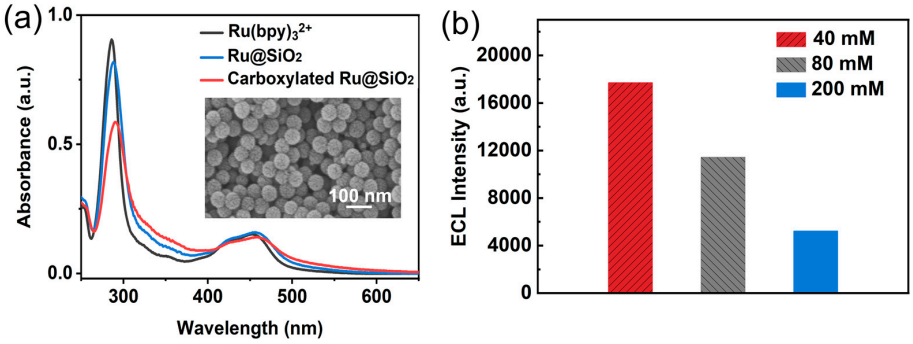

Figure 5. (**a**) UV–visible absorbance spectra of Ru(bpy)$3^{2+,}$ Ru@SiO_2 NPs and carboxylated Ru@SiO_2. (**b**) Condition optimization in preparing Ru@SiO_2 with different concentrations of Ru(bpy)3^{2+}.

3.4. Characterization of the Construction of IMBs

The construction of IMBs is characterized by both the UV–visible spectrum and the zeta potential. The UV–visible spectrum of the Ru@SiO_2–Ab_2 conjugate, obtained through EDC/NHS immobilization, is illustrated in Figure 6a. The distinctive absorption peaks of Ru@SiO_2 nanoparticles at 292 nm and 476 nm confirm the successful encapsulation of $[Ru(bpy)3]^{2+}$ within the SiO_2 nanoparticles. In the case of Ru@SiO_2–Ab_2, absorption peaks appear at 293 nm and 463 nm, with a notable decrease in the intensity of the 293 nm peak compared to Ru@SiO_2, which aligns with observations reported in the literature. There is a slight decrease observed in the zeta potential from −12.97 to −14.92 mV for MB (Figure 6b) following the immobilization of the biotinylated primary antibodies (Ab_1-biotin). This observation is consistent with a previous study, where the negative surface charge of the $Ru(bpy)_3^{2+}$–SA complex shifted further negatively after conjugation with a biotinylated CRP antibody [30]. Specifically, the Ru@SiO_2 exhibited a negative surface charge of −24.85 mV due to the presence of -COOH groups on their surfaces. Following the NHS-EDC conjugation of Ru@SiO_2 with Ab_2, the surface charge of the Ru@SiO_2 shifted positively to −18.42 mV; this is attributable to the increased number of amine groups introduced by the antibody molecules [31].

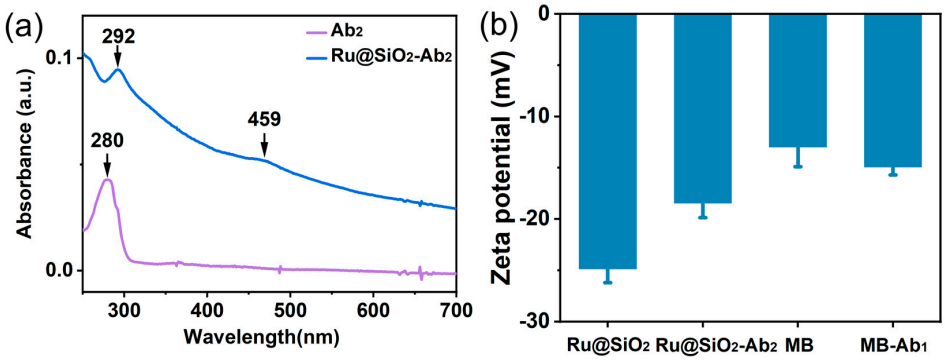

Figure 6. (**a**) UV–visible adsorption spectra of Ab_2 antibody (blue line), and Ru@SiO_2–Ab_2 (purple line). (**b**) Zeta potentials of Ru@SiO_2 and MB before and after conjugation with corresponding antibodies.

3.5. Analytical Performance of the Magneto-Immunosensor

It is evident that the use of dendrimer polymers to encapsulate Pt nanoparticles and form a film on the ITO electrode surface results in pronounced electrooxidation capability (Figure 7a) and significant enhancement of electrochemiluminescence (ECL) (Figure 7b), without compromising optical transmittance. Compared to bare ITO, the initial oxidation potential (+0.73 V) and peak potential (+0.89 V) of TPA are shifted forward by Pt-DENs/ITO. This shift is likely due to the amino groups in the Pt-DENs promoting the formation of free radicals, while the modified electrode architecture accelerates the electron and mass transfer processes. The ECL intensity at Pt-DENs/ITO in the Ru@SiO_2–TPA system is approximately 20 times greater than that observed with the bare ITO electrode. Given that the luminophores of Ru@SiO_2 are immobilized on 2.8 μm IMBs, direct electron transfer is not feasible. Nevertheless, it has been confirmed that ECL can be generated several microns above the electrode surface by employing TPA as a sacrificial oxidative–reductive coreactant [32]. This implies that immobilized Ru@SiO_2 can react with the diffusing electrogenerated TPA radicals, especially for Pt-DEN-modified MEAs. The possible ECL process of the proposed magneto-immunosensor is demonstrated in Figure 1c and the Supplementary Materials.

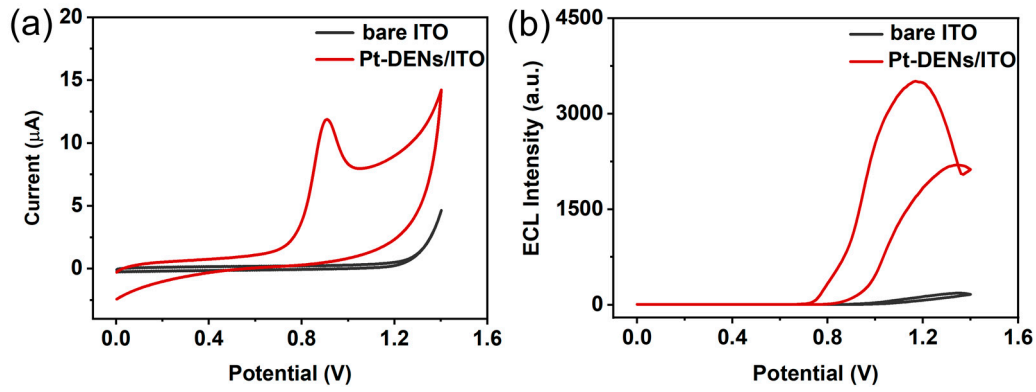

Figure 7. (**a**) CV curves of the Pt-DEN-modified ITO and bare ITO in the solution of 0.1 M PBS (pH = 7.0) in the presence of 0.16 M TPA. (**b**) ECL curves of the Pt-DENs/ITO and bare ITO electrodes in a solution of 0.1 M PBS (pH = 7.0) in the presence of 0.16 M TPA and cTnI IMBs.

The proposed ECL immunosensor was utilized to detect various concentrations of cTnI in the presence of TPA. As shown in Figure 8a, an increase in cTnI concentration from 2.5 pg/mL to 1000 pg/mL leads to a corresponding increase in ECL signals. Furthermore, the ECL intensity exhibited a favorable linear relationship with the logarithm of the cTnI concentration. The limit of detection was calculated to be 0.38 pg/mL (S/N = 3). To validate the selectivity of the platform, we investigated its ECL responses using other protein biomarkers, including creatine kinase-myocardial band (CK-MB), C-reaction protein (CRP), myoglobin (Myo), and cardiac troponin T (cTnT) as nonspecific competitors. As demonstrated in Figure 8b, the ECL intensity of cTnI at a concentration ten times lower (125 pg/mL) was significantly higher than that of the other four interference biomarkers, indicating excellent selectivity of the magneto-immunosensor for cTnI; this was partly due to effective immunomagnetic separation. Moreover, the proposed immunosensor demonstrated an outstanding detection limit for the magneto-immunoassay in comparison to other ECL research on cTnI detection (see Table 1). The ECL system, electrode materials, and analytical performances, including detection limit and linear range in the sensing systems [33–37], are compared in Table 1. In the ECL immunosensing systems, most of the antibodies were immobilized on the surface of the electrode. Very few studies have been conducted using magnetic beads as support materials and separation tools through the specific molecular recognition. For example, Zhang's group developed an ultrasensitive closed bipolar electrode–ECL (CBP-ECL) immunosensor based on a lateral flow assay

for point-of-care testing (POCT) [38]. Although acceptable sensitivity (0.4416 pg/mL) was obtained, there was a slight deficiency in selectivity. In our study, a magnetically assisted electrochemiluminescence biosensor with enhanced ECL intensity was explored by developing single-layer immunomagnetic beads (IMBs) in the vicinity of the electrode surface, as well as excellent electrode modification for the improved electrooxidation of TPA.

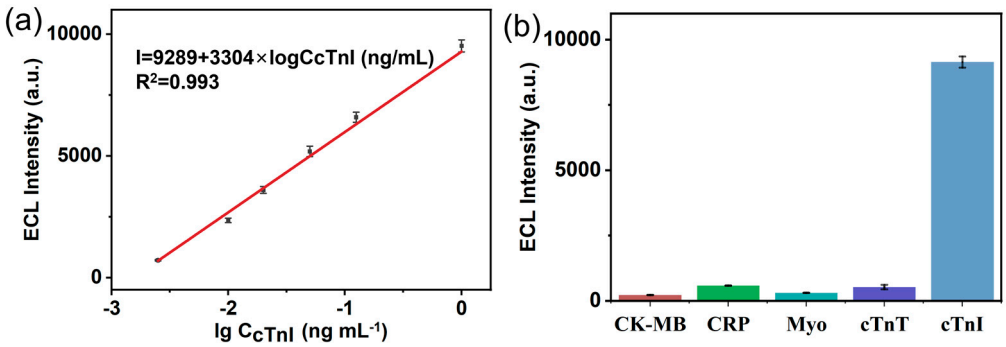

Figure 8. (**a**) Calibration curves obtained with Pt DEN-modified ITO MEAs for the analysis of cTnI in 0.1 M PBS solutions containing 0.16 M TPA. (**b**) Selectivity investigation of the proposed platform for detection of cTnI. (1.25 ng/mL), CRP (1.25 ng/mL), Myo (1.25 ng/mL), cTnT (1.25 ng/mL), and cTnI (125 pg/mL); 1.25 ng/mL CK-MB, CRP, Myo, and cTnT were used as the interferents. The error bars represent the standard deviation from three assays (n = 3).

Table 1. Comparison of the proposed magneto-immunosensor with other ECL methods for the determination of cTnI.

Electrode Material	ECL System	Linear Dynamic Range (pg/mL)	Limit of Detection (pg/mL)
Ir nanorods/Glassy carbon electrode [33]	SnS_2-Hollow polymeric spherical	1–1,000,000	0.32
Carbon ink screen-printed electrode [34]	Luminol/H_2O_2	1000–1,000,000	940
PDMS slab/ITO [35]	Horseradish peroxidase–gold nanoparticles/H_2O_2 + $Ru(bpy)_3^{2+}$/TPA	1–50,000	0.5
Screen-printed gold electrode [36]	Ru@SiO_2/TPA	1–100,000	0.81
Polyethylenimine– graphene oxide/Glassy carbon electrode [37]	Soybean peroxidase/Luminol/H_2O_2	5–30,000	3.3
Closed bipolar electrode [38]	$Ru(bpy)_3^{2+}$/L-cysteine	1–100,000,000	0.4416
Pt-DENs/ITO MEAs	Ru@SiO_2/TPA	2.5–1000	0.38

4. Conclusions

In summary, we proposed an effective and promising biomimetic chip featuring dendrimer-encapsulated Pt nanoparticle-modified biomimetic surfaces for sensitive ECL magneto-immunoassay. ITO serves as both the substrate for biomimetic nepenthes peristome microstructures and the working electrode for the ECL system. The Pt-DEN-modified ITO MEAs significantly enhanced the formation of TPA free radicals and accelerated the electron transfer process, thereby boosting ECL emission. Furthermore, the detection of cTnI at various concentrations demonstrated good linearity, with a calculated limit of detection of 0.38 pg/mL, thereby aiding in the early diagnosis and treatment of acute myocardial infarction. Furthermore, the proposed platform holds great promise for single-particle ECL imaging for the detection of various biomarkers.

Supplementary Materials: The following supporting information can be downloaded at: https://www.mdpi.com/article/10.3390/chemosensors12100214/s1, Figure S1: Design criteria for biomimetic NPS, Figure S2: Particle size distribution histograms of as-synthesized Pt-DENs. References [19,39–41] are cited in the supplementary materials.

Author Contributions: Conceptualization, Y.H. and T.W.; methodology, T.W., Y.H. and W.S.; validation, W.S. and Z.P.; formal analysis, F.S.; investigation, M.J., Z.P. and Z.X.; resources, Z.X.; data curation, W.K. and M.J.; writing—original draft, Y.H., W.K. and F.S.; writing—review and editing, W.Z. and X.-F.Y.; supervision, T.W.; project administration, Xue-Feng Yu; funding acquisition, W.Z. and X.-F.Y. All authors have read and agreed to the published version of the manuscript.

Funding: This research was funded by the National Key R&D Program of China (2023YFA0915600), National Natural Science Foundation of China (32471459, 22104148), Guangdong Basic and Applied Basic Research Foundation (2024A1515012157, 2020A1515110201, 2021A1515220156), and Shenzhen Science and Technology Research Funding (JSGG20201103153801005, ZDSYS20220527 KJZD20230923114703007), Shenzhen Medical Research Fund No. B2302028.

Institutional Review Board Statement: Not applicable.

Informed Consent Statement: Not applicable.

Data Availability Statement: The original contributions presented in the study are included in the article/Supplementary Materials. The data presented in this study are available on request from the corresponding author upon reasonable request.

Conflicts of Interest: The authors declare no conflict of interest.

References

1. Zhao, H.; Lin, Q.; Huang, L.; Zhai, Y.; Liu, Y.; Deng, Y.; Su, E.; He, N. Ultrasensitive chemiluminescence immunoassay with enhanced precision for the detection of cTnI amplified by acridinium ester-loaded microspheres and internally calibrated by magnetic fluorescent nanoparticles. *Nanoscale* **2021**, *13*, 3275–3284. [CrossRef] [PubMed]
2. Lee, T.H.; Chen, L.C.; Wang, E.; Wang, C.C.; Lin, Y.R.; Chen, W.L. Development of an electrochemical immunosensor for detection of cardiac troponin i at the point-of-care. *Biosensors* **2021**, *11*, 210. [CrossRef] [PubMed]
3. Kavetskyy, T.; Alipour, M.; Smutok, O.; Mushynska, O.; Kiv, A.; Fink, D.; Farshchi, F.; Ahmadian, E.; Hasanzadeh, M. Magneto-immunoassay of cancer biomarkers: Recent progress and challenges in biomedical analysis. *Microchem. J.* **2021**, *167*, 106320. [CrossRef]
4. Chinnadayyala, S.R.; Park, J.; Le, H.T.N.; Santhosh, M.; Kadam, A.N.; Cho, S. Recent advances in microfluidic paper-based electrochemiluminescence analytical devices for point-of-care testing applications. *Biosens. Bioelectron.* **2019**, *126*, 68–81. [CrossRef]
5. Liu, Y.; Zhang, H.; Li, B.; Liu, J.; Jiang, D.; Liu, B.; Sojic, N. Single Biomolecule Imaging by Electrochemiluminescence. *J. Am. Chem. Soc.* **2021**, *143*, 17910–17914. [CrossRef]
6. Gao, W.; Muzyka, K.; Ma, X.; Lou, B.; Xu, G. A single-electrode electrochemical system for multiplex electrochemiluminescence analysis based on a resistance induced potential difference. *Chem. Sci.* **2018**, *9*, 3911–3916. [CrossRef]
7. Chang, Y.; Wang, Y.; Zhang, J.; Xing, Y.; Li, G.; Deng, D.; Liu, L. Overview on the Design of Magnetically Assisted Electrochemical Biosensors. *Biosensors* **2022**, *12*, 954. [CrossRef]
8. Science, D.; No, S.; Chemiluminescence, A.E.; Fundamentals, F.; Edited, B.; Sojic, N.; Society, T.R.; Society, R. *Analytical Elelectrogenerated Chemiluminescence from Fundamentals to Bioassays*; Number 15; Royal Society of Chemistry: London, UK, 2020.
9. Liu, D.; Zhou, Y.; Gao, S.; Tang, Z.; La, M. Overview on the design and application of magnetically-assisted electrochemiluminescence biosensors. *Int. J. Electrochem. Sci.* **2022**, *17*, 221189. [CrossRef]
10. Sentic, M.; Milutinovic, M.; Kanoufi, F.; Manojlovic, D.; Arbault, S.; Sojic, N. Mapping electrogenerated chemiluminescence reactivity in space: Mechanistic insight into model systems used in immunoassays. *Chem. Sci.* **2014**, *5*, 2568–2572. [CrossRef]
11. Huang, C.Y.; Lin, F.Y.; Chang, C.J.; Lu, C.H.; Chen, J.K. Performance Enhancement of Electrochemiluminescence with the Immunosensor Controlled Using Magnetized Masks for the Determination of Epithelial Cancer Biomarker EpCAM. *Anal. Chem.* **2023**, *95*, 986–993. [CrossRef]
12. Valenti, G.; Fiorani, A.; Li, H.; Sojic, N.; Paolucci, F. Essential Role of Electrode Materials in Electrochemiluminescence Applications. *ChemElectroChem* **2016**, *3*, 1990–1997. [CrossRef]
13. Cheng, K.; Guo, J.; Fu, Y.; Guo, J. Active microparticle manipulation: Recent advances. *Sens. Actuators A Phys.* **2021**, *322*, 112616. [CrossRef]
14. Nilsson, J.; Evander, M.; Hammarström, B.; Laurell, T. Review of cell and particle trapping in microfluidic systems. *Anal. Chim. Acta* **2009**, *649*, 141–157. [CrossRef] [PubMed]

15. Kan, C.W.; Rivnak, A.J.; Campbell, T.G.; Piech, T.; Rissin, D.M.; Mösl, M.; Petera, A.; Niederberger, H.P.; Minnehan, K.A.; Patel, P.P.; et al. Isolation and detection of single molecules on paramagnetic beads using sequential fluid flows in microfabricated polymer array assemblies. *Lab Chip J.* **2012**, *12*, 977–985. [CrossRef] [PubMed]
16. Kitagawa, A.; Ota, M.; Watamura, T.; Tonooka, T.; Murai, Y. Microplastic particle trapping through microfluidic devices with different shaped pillars. *Chem. Eng. Sci.* **2022**, *264*, 118163. [CrossRef]
17. Chen, X.; Shojaei-Zadeh, S.; Gilchrist, M.L.; Maldarelli, C. A lipobead microarray assembled by particle entrapment in a microfluidic obstacle course and used for the display of cell membrane receptors. *Lab A Chip* **2013**, *13*, 3041–3060. [CrossRef]
18. Peng, Z.; Wu, T.; Shu, W.; Wang, Y. Facile and High-Efficiency Microbead Array Based on Biomimetic Nepenthes Peristome Surfaces. In Proceedings of the 2019 IEEE 32nd International Conference on Micro Electro Mechanical Systems (MEMS), Seoul, Republic of Korea, 27–31 January 2019; pp. 229–232. [CrossRef]
19. Peng, Z.; Chen, Y.; Wu, T. Ultrafast Microdroplet Generation and High-Density Microparticle Arraying Based on Biomimetic Nepenthes Peristome Surfaces. *ACS Appl. Mater. Interfaces* **2020**, *12*, 47299–47308. [CrossRef]
20. Rebeccani, S.; Zanut, A.; Santo, C.I.; Valenti, G.; Paolucci, F. A Guide Inside Electrochemiluminescent Microscopy Mechanisms for Analytical Performance Improvement. *Anal. Chem.* **2022**, *94*, 336–348. [CrossRef]
21. Ren, L.L.; Dong, H.; Han, T.T.; Chen, Y.; Ding, S.N. Enhanced anodic electrochemiluminescence of CdTe quantum dots based on electrocatalytic oxidation of a co-reactant by dendrimer-encapsulated Pt nanoparticles and its application for sandwiched immunoassays. *Analyst* **2017**, *142*, 3934–3941. [CrossRef]
22. Kim, Y.; Kim, J. Modification of indium tin oxide with dendrimer-encapsulated nanoparticles to provide enhanced stable electrochemiluminescence of $Ru(bpy)_3^{2+}$/tripropylamine while preserving optical transparency of indium tin oxide for sensitive electrochemiluminescence-ba. *Anal. Chem.* **2014**, *86*, 1654–1660. [CrossRef]
23. Zhao, W.R.; Xu, Y.H.; Kang, T.F.; Zhang, X.; Liu, H.; Ming, A.J.; Cheng, S.Y.; Wei, F. Sandwich magnetically imprinted immunosensor for electrochemiluminescence ultrasensing diethylstilbestrol based on enhanced luminescence of Ru@SiO2 by CdTe@ZnS quantum dots. *Biosens. Bioelectron.* **2020**, *155*, 112102. [CrossRef] [PubMed]
24. Hui, Y.; Shu, W.; Zhu, J.; Li, J.; Wu, T.; Zhou, W.; Yu, X. Pt Dendrimer-Encapsulated Nanoparticles Modified UMEAs for Electrochemiluminescence Heterogeneous Immunoassay. In Proceedings of the 2023 IEEE SENSORS, Vienna, Austria, 29 October–1 November 2023; pp. 1–4. [CrossRef]
25. Hui, Y.; Zhao, Z.; Shu, W.; Shen, F.; Kong, W.; Geng, S.; Xu, Z.; Wu, T.; Zhou, W.; Yu, X. An electrochemiluminescent magneto-immunosensor for ultrasensitive detection of hs-cTnI on a microfluidic chip. *Nanotechnol. Precis. Eng.* **2024**, *7*, 033002. [CrossRef]
26. Podešva, P.; Liu, X.; Neu, P. Single nanostructured gold amalgam microelectrode electrochemiluminescence: From arrays to a single point. *Sens. Actuators B Chem.* **2019**, *286*, 282–288. [CrossRef]
27. Cui, C.; Jin, R.; Jiang, D.; Zhang, J.; Zhu, J.J. Electrogenerated Chemiluminescence in Submicrometer Wells for Very High-Density Biosensing. *Anal. Chem.* **2020**, *92*, 578–582. [CrossRef]
28. Chen, H.; Zhang, L.; Zhang, P.; Zhang, D.; Han, Z.; Jiang, L. A Novel Bioinspired Continuous Unidirectional Liquid Spreading Surface Structure from the Peristome Surface of Nepenthes alata. *Small* **2017**, *13*, 1601676. [CrossRef]
29. Mark, S.S.; Bergkvist, M.; Yang, X.; Angert, E.R.; Batt, C.A. Self-assembly of dendrimer-encapsulated nanoparticle arrays using 2-D microbial S-layer protein biotemplates. *Biomacromolecules* **2006**, *7*, 1884–1897. [CrossRef]
30. Hong, D.; Kim, K.; Jo, E.J.; Kim, M.G. Electrochemiluminescence-Incorporated Lateral Flow Immunosensors Using $Ru(bpy)_3^{2+}$-Labeled Gold Nanoparticles for the Full-Range Detection of Physiological C-Reactive Protein Levels. *Anal. Chem.* **2021**, *93*, 7925–7932. [CrossRef]
31. Sahoo, S.L.; Liu, C.H.; Kumari, M.; Wu, W.C.; Wang, C.C. Biocompatible quantum dot-antibody conjugate for cell imaging, targeting and fluorometric immunoassay: Crosslinking, characterization and applications. *RSC Adv.* **2019**, *9*, 32791–32803. [CrossRef]
32. Voci, S.; Goudeau, B.; Valenti, G.; Lesch, A.; Jovic´, M.; Rapino, S.; Paolucci, F.; Arbault, S.; Sojic, N. Surface-Confined Electrochemiluminescence Microscopy of Cell Membranes. *J. Am. Chem. Soc.* **2018**, *140*, 14753–14760. [CrossRef]
33. Zhao, J.; Chen, X.; Wen, Y.; Tan, X.; Yuan, R.; Chen, S. Assembling inner filter effect reduced SnS2 quantum dots-based hollow polymeric spherical nanoshells for ratio electrochemiluminescence bioassay. *Biosens. Bioelectron.* **2022**, *218*, 114786. [CrossRef]
34. Du, F.; Dong, Z.; Guan, Y.; Zeid, A.M.; Ma, D.; Feng, J.; Yang, D.; Xu, G. Single-Electrode Electrochemical System for the Visual and High-Throughput Electrochemiluminescence Immunoassay. *Anal. Chem.* **2022**, *94*, 2189–2194. [CrossRef] [PubMed]
35. Cao, J.T.; Zhao, L.Z.; Fu, Y.Z.; Liu, X.M.; Ren, S.W.; Liu, Y.M. Tyramide signal amplification and enzyme biocatalytic precipitation on closed bipolar electrode: Toward highly sensitive electrochemiluminescence immunoassay. *Sens. Actuators B Chem.* **2021**, *331*, 129427. [CrossRef]
36. Hong, D.; Jo, E.J.; Kim, K.; Song, M.B.; Kim, M.G. $Ru(bpy)_3^{2+}$-Loaded Mesoporous Silica Nanoparticles as Electrochemiluminescent Probes of a Lateral Flow Immunosensor for Highly Sensitive and Quantitative Detection of Troponin I. *Small* **2020**, *16*, 2004535. [CrossRef] [PubMed]
37. Tang, M.; Zhou, Z.; Shangguan, L.; Zhao, F.; Liu, S. Electrochemiluminescent detection of cardiac troponin I by using soybean peroxidase labeled-antibody as signal amplifier. *Talanta* **2018**, *180*, 47–53. [CrossRef] [PubMed]
38. Zhan, T.; Su, Y.; Lai, W.; Chen, Z.; Zhang, C. A dry chemistry-based ultrasensitive electrochemiluminescence immunosensor for sample-to-answer detection of Cardiac Troponin I. *Biosens. Bioelectron.* **2022**, *214*, 114494. [CrossRef]

39. Zhang, L.; Dong, S. Electrogenerated chemiluminescence sensing platform using Ru (bpy) 32+ doped silica nanoparticles and carbon nanotubes. *Electrochem. Commun.* **2006**, *8*, 1687–1691. [CrossRef]
40. Zanut, A.; Palomba, F.; Rossi Scota, M.; Rebeccani, S.; Marcaccio, M.; Genovese, D.; Rampazzo, E.; Valenti, G.; Paolucci, F.; Prodi, L. Dye-doped Silica nanoparticles for enhanced ECL-based immunoassay analytical performance. *Angew. Chem. Int. Ed.* **2020**, *59*, 21858–21863. [CrossRef]
41. Valenti, G.; Rampazzo, E.; Bonacchi, E.; Petrizza, L.; Marcaccio, M.; Prodi, L.; Paolucci, F. Variable doping induces mechanism swapping in electrogenerated chemiluminescence of Ru(bpy)32+ core-shell silica nanoparticles. *J.Am. Chem. Soc.* **2016**, *138*, 15935–15942. [CrossRef]